AGU100 ADVANCING EARTH AND SPACE SCIENCE

Earth and Space Science

REVIEW ARTICLE
10.1029/2019EA000583

Special Section:
Nonlinear Systems in Geophysics: Past Accomplishments and Future Challenges

Key Points:
- This is a review of heat transport scaling theories for Rayleigh-Bénard convection
- The details of the heat transfer power-law scalings for thermal convection with and without both rotation and magnetic fields are discussed

Correspondence to:
M. Plumley,
mplumley@ethz.ch

Citation:
Plumley, M., & Julien, K. (2019). Scaling laws in Rayleigh-Benard convection. *Earth and Space Science*, *34*, 1580–1592. https://doi.org/10.1029/2019EA000583

Received 31 JAN 2019
Accepted 4 AUG 2019
Accepted article online 21 AUG 2019
Published online 11 SEP 2019

Scaling Laws in Rayleigh-Bénard Convection

Meredith Plumley[1] **and Keith Julien**[2]

[1]Institute of Geophysics, ETH Zurich, Zurich, Switzerland, [2]Department of Applied Mathematics, University of Colorado Boulder, Boulder, CO, USA

Abstract The heat transfer scaling theories for Rayleigh-Bénard convection (RBC) are reviewed and discussed for configurations with and without rotation and magnetic fields. Scaling laws are a useful tool in studying and characterizing geophysical flows as they provide a basis for extrapolation to extreme parameter regimes that remain unobtainable by current computational and experimental efforts. Specifically, power law scalings that relate the efficiency of the heat transport, as measured by the nondimensional Nusselt number Nu, to the thermal driving are pursued. Relations of the functional form $Nu \propto (Ra/Ra_c)^{\alpha}$ are considered. Given the strongly stabilizing influences of rotation and magnetic fields, thermal driving is considered in the context of the supercriticality of the system given by the ratio of the Rayleigh number Ra, measuring the thermal forcing, to the critical Ra_c, above which convection occurs. Analytical predictions for the exponent α are presented for the regimes of convection, rotating convection, and magnetoconvection, and the scalings are benchmarked against available numerical and experimental results in the accessible regimes. The exponents indicate that the thermal bottleneck to heat transport occurs within the thermal boundary layers for nonrotating RBC and the turbulent interior for rotating RBC. For magnetoconvection, a single exponent of $\alpha = 1$ is obtained for all theories and no bottleneck is identified.

1. Introduction

A primary goal of numerical simulations of planetary and stellar interiors is to produce results applicable to actual geophysical and astrophysical objects. Fluid flow phenomena occurring within these objects are typically highly turbulent, displaying a vast range of spatiotemporal scales. Indeed, the estimated Reynolds number $Re = UL/\nu$ characterizing the strength of inertial acceleration forces to viscous forces is typical extremely large, for example, $\gtrsim O(10^8)$. Here U, L respectively denote characteristic velocity and length scales and ν denotes the kinematic viscosity. As a first-order estimate, the theory of homogeneous, isotropic turbulence predicts that the ratio between the largest and smallest length scales in a turbulent flow scales as $O(Re^{3/4})$ (Pope, 2000), or $O(10^6)$ spatial degrees of freedom in a given direction for $Re = O(10^8)$. This should be contrasted with numerical simulations where limitations enforced by current computational architectures restrict the permissible degrees of freedom to $O(10^3)$ or $Re \lesssim O(10^4)$. Thus, simulated regimes remain far from being physically realistic. As computational capabilities improve, through faster machines purportedly following Moore's law (Moore, 1965), increased memory bandwidth and more efficient algorithms, simulations are on the verge of approaching degrees of freedom on $O(10^4)$ (or $Re \lesssim O(10^5)$) implying a slow progression toward the geophysical and astrophysical regimes. Nevertheless, they are still several orders of magnitude away from the expected parameter values.

Despite the aforementioned limitations, computational advances have enabled the possibility of performing multitudes of simulations to survey ranges of parameter space within moderate regimes. This has allowed numerical studies to focus on scaling laws that provide functional relationships between key diagnostics and nondimensional parameters that are widely used in fluid dynamics. Their advantage includes a reduction in the number of parameters that characterize the fluid state by defining a relationship (typically a power law) between nondimensional diagnostics and parameters. Scaling laws can be deduced either empirically, by comparing the magnitudes of terms in the governing equations with respect to an external control parameter, or theoretically, by using physical arguments to find relationships among the parameters in a physical system. A further advantage is the extrapolation of these scaling laws to study geophysical and astrophysical settings that are impossible to directly simulate. Admittedly, such extrapolations are presumed to occur within an ultimate regime so caution must be exercised due to the potential existence of unidentified flow

transitions that may invalidate the utility of the scaling law. With this caveat aside, agreement among such empirical and theoretical approaches yield a detailed understanding of the turbulent fluid states. Thus, the security in extrapolation afforded by robust scaling laws is a key benefit in geophysical investigations and has led to their wide pursuit in the field.

The pathway to understanding the high *Re* turbulent motions in geophysical and astrophysical settings is complicated. Geophysical and astrophysical fluid dynamics (GAFD) is a field that in many respects suffers from the paucity of observational data that would greatly advance our understanding. Scaling theories offer insight into force balances in the governing equations. Given that direct numerical simulations will remain far from GAFD parameter regimes for the foreseeable future, progress will demand the development of new models and perhaps sub-grid-scale parameterizations that enable greater access to the large-scale turbulent dynamics. However, both strategies should be tested and contrasted against the expectations of scalings such as heat and momentum transport. This article touches primarily on one aspect, the efficiency of heat transport. It is highly influenced by the varying constraints of rotational and magnetic forces and often involves several transitions in flow morphology, sometimes realized with transitions in the heat transport exponents. Understanding the source of variability in such exponents can also lead to an understanding of the important force balances in the equations and enable model reduction based on the identified key dynamics. These reductions can take the form of improved parameterizations of key components of the flow, for instance, the use of a convective parametrization based on mixing length theory for the evolution of stellar structure (Böhm-Vitense, 1958). However, an improved understanding between exponents and related transitions in the flow may also provide further opportunities for parameterizations of the high *Re* regime.

The desired functional form of the scalings varies by application, but they typically relate an input parameter to an output value. Examples include the relationship between thermal forcing and heat transfer efficiency for nonrotating convection studies (Howard, 1972; Kraichnan, 1962), velocity and rotational strengths (Cheng et al., 2015; Ecke & Niemela, 2014; King & Aurnou, 2013; Plumley et al., 2017; Rubio et al., 2014), or the typical velocity and magnetic field strength for a given heat flux in dynamo studies (Christensen, 2010; Davidson, 2013). Another alternative is to uncover dominant force balances that may be utilized for model reduction or parameterizations appropriate for geophysical and astrophysical settings (Aubert, 2019; Julien et al., 2006).

This article focuses on the theories and verification of scaling laws for heat transfer within simplified convection models. Specifically, thermally driven Boussinesq convection is considered in a plane-parallel layer. The model is ideal for the application of both analytical approaches and empirical exploration because of the fundamental nature of both its configuration and the governing equations that describe fluid motions. The influence of rotation and magnetic fields is also considered given their ubiquity in many geophysical and astrophysical settings, including planetary and stellar interiors (Jones, 2007). The motivating argument for studying the scaling laws in this simplified system is to investigate the fundamental dynamics of the problem in a format that allows for a progression of understanding as more complexities are added. For instance, comparative studies of the influence of heat transport in the presence and absence of rotation and/or magnetic fields. This type of hierarchical approach in establishing scaling laws provides an excellent opportunity for collaborative efforts involving laboratory, computational, and theoretical studies (Aurnou et al., 2015). Specifically, finding and calibrating scaling laws relies on a combination of analytical reasoning, theoretical bounding arguments, and numerical and experimental simulation. Implicit here is the need for the engagement of a wide variety of analysis tools brought together by engaging a diverse spectrum of researchers. The focus here is on the scaling of the heat transfer as a function of the thermal driving of the system. This scaling is a prominent topic due to its sensitivity to the flow morphology and because it is one of the primary metrics in laboratory and numerical studies. Of course, geophysical and astrophysical objects are not completely characterized by plane layer convection, even with the addition of rotation and magnetic fields. The search for scaling laws that apply in more complex settings, such as in sphere or spherical shell geometries or with compressibility are typically guided by numerical simulations (e.g., Christensen & Aubert, 2006; Davidson, 2013; Gastine et al., 2016). This review presents an analysis of scaling laws for the heat transfer in plane layer thermally driven Boussinesq convection in section 2, with the addition of rotation in section 3, and magnetoconvection in section 4.

2. Rayleigh-Bénard Convection

Thermally driven convection is a conceptually simple paradigm for studying heat transfer as it might apply in planetary and stellar interiors. The typical setup includes a container of fluid heated from below and cooled from above. In the laboratory cylindrical containers are common whereas Cartesian boxes with periodic sidewalls are common for numerical simulations. For a sufficiently high temperature difference ΔT between the top and bottom, buoyancy will drive a overturning flow known as Rayleigh-Bénard convection (RBC). RBC flow is described by the incompressible Navier-Stokes equations under the Boussinesq approximation

$$\frac{\partial \boldsymbol{u}}{\partial t} + \boldsymbol{u}\cdot\nabla\boldsymbol{u} = -\frac{1}{\rho_0}\nabla P + \nu\nabla^2\boldsymbol{u} + g\alpha_T T\hat{\boldsymbol{z}}, \tag{1}$$

$$\nabla\cdot\boldsymbol{u} = 0, \tag{2}$$

$$\frac{\partial T}{\partial t} + \boldsymbol{u}\cdot\nabla T = \kappa\nabla^2 T \tag{3}$$

with an equation of state

$$\rho = \rho_0(1-\alpha_T(T-T_0)). \tag{4}$$

Here u is the velocity vector, P is the modified pressure, ρ is the fluid density with reference value ρ_0, T is the temperature with reference value T_0, ν is the kinematic viscosity, κ is the thermal diffusivity, α_T is the thermal expansion coefficient, and g is the acceleration due to gravity, which, as considered here, is commonly aligned with the vertical axis $\hat{z}$. This large array of parameters may be greatly reduced using dimensional analysis to produce two nondimensional parameters: the Rayleigh number $Ra = g\alpha_T\Delta T H^3/(\kappa\nu)$ measuring the degree of thermal forcing and Prandtl number $Pr = \nu/\kappa$ detailing thermometric properties of the fluid. The onset of convection can be expressed by the critical $Ra_c = c$. Here c is a constant that depends on the boundary conditions applied and is typically $O(10^3)$ (Chandrasekhar, 1961; Cross & Hohenberg, 1993).

One of the key diagnostics for RBC flow is the Nusselt number Nu, which measures the dimensionless heat transfer rate through the ratio of the total heat flux q to the heat flux resulting from conduction alone. The Nusselt number is defined by $qH/\kappa\Delta T$, and it is an important diagnostic of the underlying convective flow. Of particular interest is the functional dependence of Nu with respect to Ra and Pr that encodes the underlying physics of the fluid flow, that is, $Nu = Nu(Ra, Pr)$. Specifically, at sufficiently supercritical Rayleigh numbers, $Ra \gg Ra_c$, a commonly observed functional form is the power law functional

$$Nu = c_1 Pr^{\gamma}\left(\frac{Ra}{Ra_c}\right)^{\alpha} \tag{5}$$

where the exponents

$$\alpha = \frac{\partial \ln(Nu)}{\partial \ln(Ra)}, \qquad \gamma = \frac{\partial \ln(Nu)}{\partial \ln(Pr)} \tag{6}$$

are understood to be constant over a range of Ra and Pr, respectively. Here c_1 is a constant. This functional form (Howard, 1972) is based on the supercriticality of the convection, where the supercriticality expressed as Ra/Ra_c is a relevant parameter for indicating that a flow is fully in the convective, turbulent regime. It is necessarily bounded away from the onset of convection. In laboratory and numerical experiments, once the thermometric properties of the fluid (such as Pr) and geometry of the setup are set, the critical Ra_c is a constant value, independent of all other parameters, and changing the Rayleigh number is reduced to varying ΔT between the boundaries or the power input at the lower boundary.

The Prandtl number defining the fluid type for use in the laboratory varies over the range $O(10^{-3})$–$O(10^5)$ with $Pr \approx 0.004$ (for liquid sodium), 0.025 (mercury), 0.7 (gases), 3–10 (water), 5–50 (silicon), and 50–10^5 (heavy oils). In geophysical and astrophysical settings, the Prandtl number values can vary from the solar interior at $Pr = O(10^{-6})$ (Miesch, 2005) to mantle convection, where $Pr = O(10^{23})$. In the numerical setting there are various options for exploring the range of Pr by taking the appropriate limits of the Navier-Stokes equations. The low Prandtl number limit (Thual, 1992) presents a particularly unique challenge numerically as the dissipation length scales, separated by a factor of the Prandtl number, play important roles in the heat

transport and thus demand increasingly prohibitive spatiotemporal resolution requirements. By contrast, the infinite Prandtl number limit becomes inertia free and allows for a straightforward simplification of the governing system (Constantin & Doering, 1999; Grossmann & Lohse, 2001; Wang, 2004). Experimental investigations of the scalings for Prandtl number dependence are more challenging to obtain than studying the *Ra* response due to several mechanical and thermal factors. These include a lack of detailed coverage of the range spanned by the working fluids as well as issues in controlling the thermometric properties as a function of temperature and pressure. The *Pr* dependence has been investigated (e.g., Ahlers & Xu, 2001; Grossmann & Lohse, 2002; Roche et al., 2002; Stevens et al., 2011); however, due to the difficulties most experimental studies focus on the scaling of *Ra* for a fixed $Pr = O(1)$ fluid and those are the results we focus on here.

For laboratory experiments and numerical simulations α is dependent on internal parameters that are inherently fixed by geometry and boundary conditions. The difference in boundary conditions, such as stress free versus no slip, can be more readily explored in numerical settings. One difference between the experimental and simulation data is the effect of the sidewalls in the physical experiments. Further details on the sidewall effects are presented in Ahlers et al. (2009), Liu et al. (2018), and Kunnen et al. (2013).

Despite the simplifying reductions of the RBC configuration it remains difficult to simulate numerically and investigate experimentally in geophysically relevant parameter regimes. Therefore, the focus for these approaches has been primarily on finding empirical scaling laws that hold in the currently accessible region of parameter space, that is, $Ra \lesssim 10^{14}$ (He et al., 2012). Fortunately, theoretical predictions form a foundation upon which empirically deduced laws may be understood. Many can be deduced based on physical constraints on q and the dimensional terms within (5). Specifically, upon rearrangement, one obtains

$$q \propto \left(\frac{\kappa \Delta T}{H}\right)\left(\frac{\nu}{\kappa}\right)^{\gamma}\left(\frac{g\alpha_T \Delta T H^3}{\kappa \nu}\right)^{\alpha}. \tag{7}$$

Physical constraints then result in algebraic constraints for the exponents α, γ. In turbulent regimes, occurring at sufficiently large *Ra*, it is observed that the fluid layer is characterized by an isothermal turbulent fluid interior sandwiched between thermal boundary layers of depth λ and temperature drop $\Delta T/2$. Within the turbulent interior, where dissipative processes are subdominant, the total heat flux q has no functional dependence on ν, κ. From (7) this results in the algebraic constraints $\gamma + \alpha = 1$ and $\gamma - \alpha = 0$, which is satisfied by $\alpha = \gamma = 1/2$. Priestley (1959) argued that the turbulent interior severs direct communication between the two laminar boundary layers. Thus, q is independent of the layer depth H resulting in the algebraic constraint $3\alpha - 1 = 0$ or $\alpha = 1/3$. Malkus (1954) argued that in an asymptotic turbulent state the thermal boundary layers are in a state of marginal stability, that is, $Ra_{\lambda c} \equiv Ra_c$, where the λ subscript denotes the value in the thermal boundary layer. Thus, given a temperature drop $\Delta T_\lambda = \Delta T/2$ the boundary layer Rayleigh and Nusselt numbers satisfy

$$\frac{Ra_\lambda}{Ra_{\lambda c}} = \frac{1}{2}\left(\frac{\lambda}{H}\right)^3 \frac{Ra}{Ra_c} \equiv 1, \quad Nu_\lambda = 2\left(\frac{\lambda}{H}\right) Nu \equiv 1, \quad \Rightarrow \quad Nu = \frac{1}{2}\left(\frac{Ra}{2Ra_c}\right)^{1/3}. \tag{8}$$

Thus, as with Priestley, $\alpha = 1/3$.

A key question is which region, the boundary layer or interior, acts as the thermal bottleneck and throttles the heat flux. The straightforward answer is that the bottleneck occurs in whichever region minimizes α. Given $1/3 < 1/2$ the above theoretical arguments would imply that if the turbulent state has laminar boundary layers, then they would be the thermal bottleneck that controls the observed heat transport scalings. However, others have argued or inferred from asymptotic theories (Kraichnan, 1962; Spiegel, 1971) that the boundary layers become turbulent in the asymptotic limit $Ra \to \infty$ such that the heat transport efficiency matches the interior $\alpha = 1/2$ prediction. If this is not the case then the boundary layers remain laminar (or subturbulent) and its diffusive properties are presumed to dominate.

Alternative exponents and selection mechanisms have also been proposed. Shraiman and Siggia (1990) deduce a result of $\alpha = 2/7$ by incorporating arguments for a sheared thermal boundary layer due to the existence of large-scale circulations. However, this scaling law appears to exist in an intermediate regime suitably described by a composite scaling law (Grossmann & Lohse, 2002). Grossmann and Lohse (2002) deduce an array of scaling exponents that result by identifying the regions of *Ra*-*Pr* parameter space

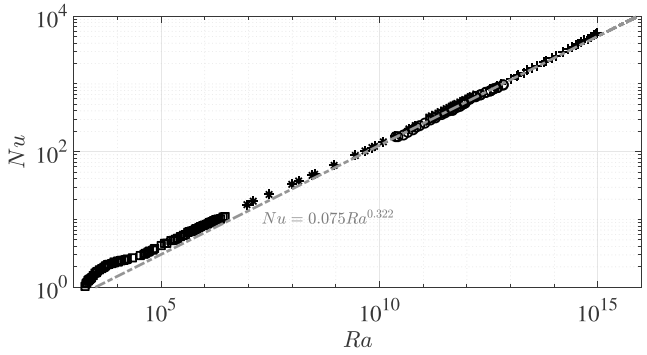

Figure 1. The Nusselt number results from several experiments over a range of Ra. The dashed line shows $Nu = 0.075\,Ra^{0.322}$, a fit from Cheng et al. (2015) based on their data for $Ra \geq 10^{10}$. The data are from laboratory experiments in water with $Pr \in [4-7]$ and are marked by squares (Rossby, 1969), asterisks (Funfschilling et al., 2005), triangles (Sun et al., 2005), circles (Cheng et al., 2015), and plus signs (He et al., 2012).

where the dominant contribution to the viscous and thermal dissipation rates arise from differing combinations of the boundary layers (viscous and thermal) and the turbulent interior. Deduced exponents include $\alpha \in (1/5, 2/3)$.

Investigations of theoretically deduced asymptotic scaling laws for Nu have been complemented by laboratory experiments and numerical simulations over accessible ranges of Ra (see figure 1). To date, the most extensive laboratory experiments in water by He et al. (2012) for Ra up to 10^{15} appear to yield a 0.31 scaling law for $Ra < 10^{13}$ with a higher scaling of 0.38 for $10^{13} < Ra < 5 \times 10^{14}$. Claims have been made for an ultimate heat transport scaling law if logarithmic corrections are accounted for (Ahlers et al., 2017; He et al., 2012; Zhu et al., 2018). However, Doering et al. (2018) argued that the data remains consistent with the 1/3 exponent with no discernible or systematic trend indicating a transition to an ultimate scaling regime. Computational limits have restricted the explorable parameter space to $Ra \lesssim 10^{12}$ in three dimensions and reported exponents support scaling exponents $\alpha \leq 1/3$ consistent with laboratory experiments in this range (Chillà & Schumacher, 2012).

To circumvent the restrictive Ra range, there have been several novel studies that probe transport scalings in systems with different configurations from the classical Rayleigh-Bénard setting of fixed temperature or fixed power input at the boundaries. Examples include working with gases at specific high temperatures and pressures that allows an extended range of $Ra \leq 10^{17}$ (Niemela et al., 2000) or altering the system to overcome the thermal boundary bottleneck (Bouillaut et al., 2019; Lohse & Toschi, 2003). Indeed, the latter technique has revealed the existence of an ultimate regime with $\alpha = 1/2$ heat transport scaling law.

Upper bounds on Nu in the limit $Ra \to \infty$ deduced based on rigorous applied analysis of the incompressible fluid equations provide an alternative approach to physically deduced scaling exponents (Tobasco & Doering, 2017). To date, the $\alpha = 1/2$ exponent is only ruled out for two-dimensional RBC with stress-free boundary conditions where it has been demonstrated $Nu \leq 0.2891 Ra^{5/12}$ (Whitehead & Doering, 2011). We note that such results are achieved through the numerical solution of the background field variational problem formulated by Doering and Constantin (1996).

3. RBC With Rotation

The RBC paradigm can be more closely connected to GAFD flows by the inclusion of rotation and/or magnetic fields. In this section we discuss the inclusion of rotation alone. In the canonical setup the RBC system is rotated around the vertical axis with angular velocity Ω. The addition of system rotation requires the inclusion of the Coriolis force in the governing momentum equation (1) such that

$$\frac{\partial \boldsymbol{u}}{\partial t} + \boldsymbol{u}\cdot\nabla\boldsymbol{u} + 2\Omega\boldsymbol{z}\times\boldsymbol{u} = -\frac{1}{\rho_0}\nabla P + \nu\nabla^2\boldsymbol{u} + g\alpha_T T\hat{\boldsymbol{z}}. \tag{9}$$

This gives rise to an additional timescale in the flow, the rotational timescale. This is expressed through an additional group of nondimensional parameters: the Ekman number $E = \nu/2\Omega H^2$ and the convective Rossby number $Ro = \sqrt{Ra/PrE} = \sqrt{g\alpha_T \Delta T/H}/2\Omega$, which define the relative importance of rotation to viscous forces and thermal forcing, respectively. For comparison, the Earth's liquid outer core is characterized by $E \approx 10^{-15}$, $Ro \approx 10^{-6}$, and $Re = Ro/E = 10^8$; Jupiters interior is characterized by $E \approx 10^{-19}$, $Ro \approx 10^{-9}$, and $Re = 10^{10}$; and its moon Ganymede by $E \approx 10^{-13}$, $Ro \approx 10^{-5}$, and $Re = 10^8$ (Schubert & Soderlund, 2011). This implies the presence of fast inertial waves with nondimensional frequencies of $O(Ro^{-1})$ and thin Ekman layers of $O(E^{1/2}H)$ that further complicate the study of turbulent flows.

Similar to nonrotating RBC, a major focus is the scaling of the heat transfer as a function of the thermal input, rotation, and fluid properties, that is, $Nu = f(Pr, Ra, E)$. As with nonrotating convection, the goal is to understand the heat transfer in a geophysically relevant parameter regime, where the system is forced past the onset of convection. In rotating convection, the critical Rayleigh number is a function of the rotation such that $Ra_{c_r} = c_r E^{-4/3}$(Chandrasekhar, 1961). Here c_r is a constant dependent on geometry and mechanical

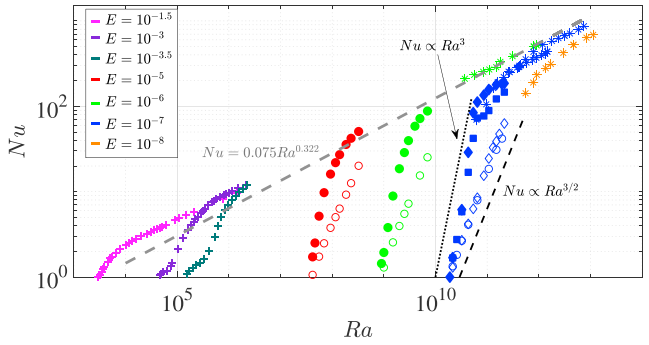

Figure 2. The Nusselt number results from both laboratory experiments in water with $Pr \approx 7$ and numerical simulations with $Pr = 7$. Laboratory experiments are marked as plus signs (Rossby, 1969) and asterisks (Cheng et al., 2015). Numerical simulations are marked as circles (Stellmach et al., 2014) and diamonds (Plumley et al., 2016). The gray diagonal line $Nu = 0.075Ra^{0.322}$ (Cheng et al., 2015) is a fit for nonrotating convection and is included to facilitate comparison with figure 1. The filled (open) symbols depict results with no-slip (stress-free) boundaries at the top and bottom plates. The black dashed line with slope $Nu \propto Ra^{3/2}$ shows the stress-free scaling result and the black dotted line shows $Nu \propto Ra^3$.

boundary conditions. This indicates that rotation inhibits convection such that stronger thermal forcing is required to drive convective motions as the rotation rate increases.

Figure 2 illustrates the influence of rotation on heat transport in the Nusselt-Rayleigh plane. A comparison with Figure 1 demonstrates that at comparable Ra the values of Nu are lower than those realized for nonrotating convection. The latter lie along the gray dashed line showing the best fit (Cheng et al., 2015) for nonrotating convection. This observation is related to the dependence of the critical Ra_{c_r} on E, indicating the strong stabilizing effect of rotation, which delays convective onset. As such, rotating convective fluids have significantly lower supercriticalities compared to nonrotating convection at equivalent Ra. Additionally, the comparison of the figures shows the more limited range of Ra achieved for rapidly rotating convection at fixed E before transitioning to the buoyancy dominated regime where the influence of the Coriolis force becomes negligible. This limitation reduces the interval over which rotational scaling laws may be explored and thus presents a major challenge for experimentally probing rotationally constrained convection. Moreover, given the computational difficulties required to remain in the low-Ro, low-E regime, it is presently also not possible to achieve the same levels of supercriticality as in the nonrotating convective case. Hence, Ra/Ra_{c_r} and the resultant Nusselt numbers are closer to the onset value of 1. However, while the range of validity for the scaling law theories is thought to lie significantly away from convective onset, simulations have shown that fluid motions in rapidly rotating flows becomes vigorous as soon as the flow becomes unstable (Busse, 1981; Julien et al., 2012). Thus, scaling laws have been observed even at relatively low supercriticality. The asymptotic analysis and results showing convergence to scaling laws (Plumley et al., 2017) suggest that it is appropriate to benchmark theoretically deduced scalings with the numerical experimental results in the less supercritical, but accessible regime.

The functional form

$$Nu \propto Pr^{\gamma}\left(\frac{Ra}{Ra_{c_r}}\right)^{\alpha}, \tag{10}$$

can now be expressed

$$Nu = c_2 Pr^{\gamma} Ra^{\alpha} E^{4\alpha/3}, \tag{11}$$

where the heat flux now varies additionally with the rotation of the system due to the critical Ra_{c_r}. Here c_2 is a constant. This functional form is again based on the supercriticality of the convection and has a key difference from the non rotating case since the critical Ra_{c_r} depends on the rotation through a factor of $E^{-4/3}$. The above functional form therefore provides one way of encoding this into the scalings. Thus, for the rotating case, the important parameter for determining if a flow is in the convective, turbulent regime is the supercriticality parameter $RaE^{4/3}$, often referred to as the reduced Rayleigh number. Alternative functional forms for the scaling relationship do exist, such as separate exponents for Ra and E. However, asymptotic methods and numerical simulations performed at low Rossby numbers appear to support the supercriticality dependence between Ra and E as the dominant scaling and hence endorses the form provided in (11) (Kunnen et al., 2016; Plumley et al., 2016; Stellmach et al., 2014). An indication for the failure of (11) would be that the prefactor c_2 perceived to be constant will develop a strong dependency on E, thus providing an a posteriori check. On this point, we refer the reader to the discussion at the end of this section.

The heat transfer relation can be expressed as

$$q \propto \left(\frac{\kappa \Delta T}{H}\right)\left(\frac{\nu}{\kappa}\right)^{\gamma}\left(\frac{g\alpha_T \Delta T H^3}{\kappa\nu}\right)^{\alpha}\left(\frac{\nu}{2\Omega H^2}\right)^{4\alpha/3}. \tag{12}$$

Theoretical arguments similar to those applied to RBC now apply. The picture in Priestley (1959) of a bulk interior solution independent of H now implies that $1 = 3\alpha - 8\alpha/3$ resulting in $\alpha = 3$. The constraint of

Malkus (1954) of a marginally stable thermal boundary layer implies that the boundary layer Rayleigh and Nusselt numbers satisfy, given $Ra_{\lambda c_r} = c_r E_\lambda^{-4/3}$,

$$\frac{Ra_\lambda}{Ra_{\lambda c_r}} = \left(\frac{\Delta T_\lambda}{\Delta T}\right)\left(\frac{\lambda}{H}\right)^{1/3}\frac{Ra}{c_r E^{-4/3}} \equiv 1, \quad Nu_\lambda = \left(\frac{\Delta T}{\Delta T_\lambda}\right)\left(\frac{\lambda}{H}\right)Nu \equiv 1, \quad \Rightarrow \tag{13}$$

$$Nu = \left(\frac{\Delta T_\lambda}{\Delta T}\right)^2\left(\frac{RaE^{4/3}}{c_r}\right)^3. \tag{14}$$

Here ΔT_λ denotes the temperature drop over the thermal boundary layer depth λ. The above relations then provide a scaling exponent of 3 that is equivalent to Priestley's or Malkus' result, if and only if, $\Delta T_\lambda \sim \Delta T$. However, recent results have established that the normalized temperature drop $\Delta T_\lambda/\Delta T$ is a decreasing function of Ra/Ra_{c_r} (Julien et al., 2012). This implies that the exponent of 3 provides an upper bound scaling.

Within the turbulent interior the constraint of no functional dependence on ν, κ implies $0 = \gamma - \alpha + 4\alpha/3$ and $0 = 1 - \gamma - \alpha$, resulting in $\alpha = 3/2, \gamma = -1/2$. Given the inequality $3/2 < 3$, it follows that the rotating turbulent interior is the thermal bottleneck that throttles the heat transport, such that

$$Nu = c_2 Pr^{-1/2} Ra^{3/2} E^2. \tag{15}$$

This is *diametrically* opposite to the nonrotating case where the equivalent inequality $1/2 > 1/3$ indicates that the thermal bottleneck is the thermal boundary layers. A fact that has greatly hindered the pursuit of an ultimate heat transport state in nonrotating convection. By contrast the turbulent throttling of the heat transport in rotating convection makes its observation a reality.

The ability to investigate the foregoing scaling theories presents a substantial challenge for both laboratory experiments and numerical simulations in the rapid rotation limit where $Ra \to \infty$ while $Ro, E \ll 1$. In this limit, the former is challenged by the loss of thermal control due to uncontrolled sidewall heat losses and corruption by centrifugal buoyancy effects (Cheng et al., 2018; Horn & Aurnou, 2018). DNS of the governing equations are challenged by the temporal constraint of resolving fast inertial waves and, when present, the spatial constraint of resolving Ekman boundary layers (Stellmach et al., 2014). Due to these challenges, typical values for both approaches are limited to $E \gtrsim 10^{-7}$ and $Ra \lesssim 10^{12}$. The Rossby number is limited as well by its relation to E and Ra such that the Rossby numbers achievable are typically $Ro \gtrsim 10^{-2}$ (Cheng et al., 2015). Current efforts to build larger laboratory tanks should extend this range (Cheng et al., 2018).

Asymptotic methods have provided an alternative avenue to investigate the rapidly rotating limit in parameter regimes relevant for geophysical flows (Julien & Knobloch, 2007). Specifically, the approach takes advantage of the small size of the rotation parameters E and Ro to derive a new set of reduced equations valid in the limit of $E \downarrow 0$. The equations describe the nonhydrostatic quasi-geostrophic evolution of fluid motions, that is, the evolution of fluid motions under geostrophy—a pointwise balance between the Coriolis and pressure gradient forces. The reduction benefits from increased numerically tractability by neglecting asymptotically unimportant dynamics in the flow. The models have shown high levels of quantitative agreement in comparison with DNS and experimental results in the overlaping region of $E \sim 10^{-7}$ (Stellmach et al., 2014; Plumley et al., 2016). They have also been useful in mapping the distinct flow morphologies and heat transfer within the low E parameter space (Julien et al., 2012; Plumley et al., 2017; Rubio et al., 2014). Notably, a dissipation-free scaling exponent of $\alpha = 3/2$ is observed by both asymptotic models and DNS for turbulent flow in the presence of stress-free boundaries.

Comparison of the observed exponents achievable by numerical simulations and laboratory data (Figure 2) also requires the discussion of an important caveat: the influence of mechanical boundary conditions. Linear theory (Chandrasekhar, 1961; Niiler & Bisshopp, 1965) and asymptotic theory (Julien & Knobloch, 1998) indicate a diminishing distinction between no-slip and stress-free boundary conditions in the rapidly rotating limit $E \to 0$. This is purported to occur as a consequence of the diminishing role of Ekman pumping resulting vertical velocities of $O(E^{1/2}H(\hat{\boldsymbol{z}} \cdot \nabla \times \boldsymbol{u}))$ in the presence of a no-slip bounding surface. However, recent efforts in the laboratory (Cheng et al., 2015) have shown that pumping gives rise to an enhancement in heat transport that results in measured exponents greater than 3. In fact, Cheng et al. (2015) have demonstrated that the heat transport exponent continues to increase as $E \downarrow 0$ (see Figure 3a). A clear distinction is thus observed between the heat transport in the presence of stress-free or no-slip boundary conditions.

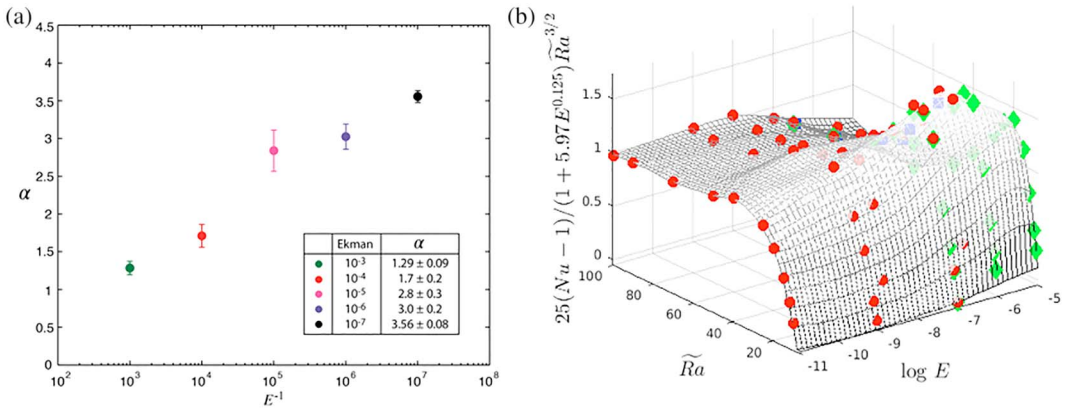

Figure 3. (a) The heat transfer scaling exponents α as a function of Ekman number for a combination of laboratory experiments and numerical simulations with $Pr \approx 7$ and no slip boundary conditions at the top and bottom boundaries. The scaling increases as E is lowered, indicating that no clear asymptotic scaling behavior has been found. This figure has been reproduced from Cheng et al. (2015). (b) The surface of $Nu(\widetilde{Ra}, \log_{10}E)$ from numerical heat transfer results using no slip boundaries and $Pr = 1$ and normalized using (16) shows the agreement with the empirical fitting and the complicated dependence on both Ra and E. The fit incorporates a prefactor of $(1 + P(E))$ where $P(E)$ is a function of the Ekman number that accounts for the functional dependence of the scaling on E, as shown in (a). This surface is reprinted from Plumley et al. (2017). The use of $\widetilde{Ra} = RaE^{4/3} \propto (Ra/Ra_{c_r})$ rather than Ra improves the clarity of the plot. Data for the asymptotic model from Plumley et al. (2016) are denoted by (red) circles, and DNS data are included for fixed Ra (blue, squares) from Kunnen et al. (2016) and fixed E (green, diamonds) from Stellmach et al. (2014).

Figure 2 shows the difference in heat transfer due to boundary condition as indicated by filled (no slip) and open (stress free) symbols. Stellmach et al. (2014); Julien et al. (2016) have demonstrated that this effect occurs as a transition within an $O(E^{1/3}H)$ thermal-wind layer sandwiched between adjacent an $O(E^{1/2}H)$ Ekman layers and the fluid interior. The interval of the transition is found to be finite in that the heat transport ultimately resettles to a pretransition exponent but with a significantly enhanced prefactor (Plumley et al., 2016; demonstrated in Figure 3b), which illustrates a transition between regimes where Ekman pumping effects are negligible and dominant (Julien et al., 2016; Plumley et al., 2016). Ultimately, when Ekman pumping is negligible heat transport returns to the dissipation-free scaling law. This suggests the existence of a more complex 2-D surface in $Nu(E, Ra)$ parameter space (Kunnen et al., 2016; Stellmach et al., 2014). For $E < 10^{-7}$ and $Pr = 1$ fluids, Plumley et al. (2017) suggested that the surface can be expressed as

$$Nu - 1 \propto (1 + P(E))(RaE^{4/3})^{3/2} \tag{16}$$

indicating the dissipation-free scaling law is enhanced by Ekman pumping by the multiplicative prefactor $(1 + P(E))$ where $P(E) \approx 5.97E^{1/8}$ was fit empirically with their numerical simulations, as shown in Figure 3b. This indicates a singular transition in the sense that its dependence on supercriticality has an inverse relationship with E; that is, it is increasingly delayed and moves to infinity as $E \to 0$. The fact that this effect is observed close to onset further highlights the moderate nature of E presently achieved. A precise understanding of this transition thus remains an open question that awaits further interrogation.

Efforts to provide upper bounds on heat transport scaling laws have only been successfully applied to the reduced asymptotic equations appropriate for stress-free boundary conditions and give $Ra^{3/2} \lesssim Nu \lesssim Ra^3$ (Grooms, 2015; Grooms & Whitehead, 2014). A similar analysis on the reduced asymptotic equations that includes the effects of Ekman pumping associated with no-slip boundaries still remains an open problem as does the direct application of upper bound theory to the incompressible equations.

4. RBC With an Imposed Magnetic Field

Another step in complexity toward GAFD modeling incorporates magnetic fields into the system. Most planetary and stellar bodies either possess or have possessed a large-scale magnetic field. It is now accepted that the turbulent convective motions in the electrically conducting interiors of planets and stars are a primary source for generating and sustaining the large-scale magnetic fields, via the so-called dynamo action (Jones, 2011). Here, turbulent motions u of an electrically conducting fluid generate a magnetic field B, which in turn feedback and influence fluid motions. This is appropriately captured by the inclusion of the magnetic

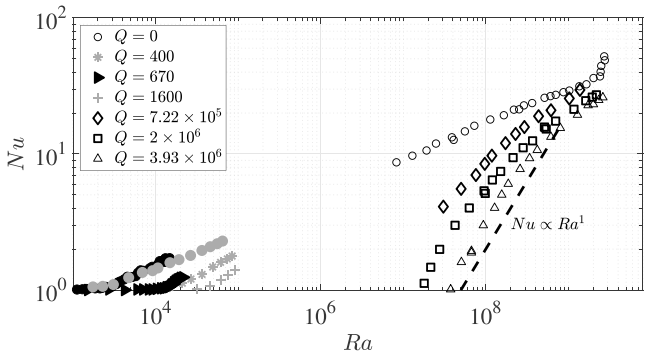

Figure 4. Magnetoconvection experimental results varying Q in mercury with $Pr = 0.025$ (open symbols) from Cioni et al. (2000), in a sodium potassium alloy with $Pr \approx 0.02$ (gray symbols) from Burr and Müller (2001) and in liquid gallium with $Pr = 0.023$ (filled black symbols) from Aurnou and Olson (2001). Here the dashed black line shows $Nu \propto Ra^1$ to guide the eye in comparison with theoretical predictions.

induction equation detailing field generation and the Lorentz body force term arising from the magnetic field and back reacts onto fluid motions. Alterations and additions to (1)-(4) are now given by

$$\frac{\partial \boldsymbol{u}}{\partial t} + \boldsymbol{u} \cdot \nabla \boldsymbol{u} = -\frac{1}{\rho_0}\nabla P + \nu \nabla^2 \boldsymbol{u} + g\alpha_T T \hat{\boldsymbol{z}} + \frac{1}{\mu \rho_0}(\nabla \times \boldsymbol{B}) \times \boldsymbol{B}, \tag{17}$$

$$\frac{\partial \boldsymbol{B}}{\partial t} + \boldsymbol{u} \cdot \nabla \boldsymbol{B} = \boldsymbol{B} \cdot \nabla \boldsymbol{u} + \eta \nabla^2 \boldsymbol{B}, \tag{18}$$

$$\nabla \cdot \boldsymbol{B} = 0. \tag{19}$$

Here μ and η represent the vacuum permeability and magnetic diffusivity of the fluid.

While a self-sustaining large-scale dynamo is the more applicable setting to investigate for geophysical and astrophysical objects, its regime of operation ultimately presents many prohibitive challenges for numerical and laboratory investigations. Principle among these is that dynamos typically operate in a regime of extremely low magnetic Prandtl number $Pm = \nu/\eta = O(10^{-6} - 10^{-5})$ that characterizes liquid metals such as gallium and sodium. When combined with the fact that the instability leading to field generation occurs for magnetic Reynolds $Rm = UH/\eta = O(10-100)$ this results in unachievable Reynolds numbers $Re = Rm/Pm$. For the geodynamo, the liquid iron outer core is characterized by $Pm = 10^{-6}$, indicating a transitional $Re \approx 10^8$. Invariably, despite many heroic efforts, numerical simulations must substantially increase Pm to achieve dynamo action and laboratory experiments have yet to either produce dynamo action (Lathrop & Forest, 2011; Zimmerman et al., 2014) or sustain a large-scale dynamo (Berhanu et al., 2010). Thus, the dynamo process is highly complex and the intimate details such as the impact of field strength remain to be elucidated (Fauve & Petrelis, 2003; Tobias, 2019). We note that alternative approaches for uncovering the scalings or balances are currently being pursued for the dynamo problem (e.g., Aubert, 2019; Calkins et al., 2015; Cattaneo & Hughes, 2006; Davidson, 2013; Gastine et al., 2016; Guervilly et al., 2019; Tilgner, 2012).

The focus here is on magnetoconvection, that is, the inclusion of an imposed magnetic field and by extension the impact of field strength. While all the results up to this point have been in liquid water ($Pr \approx 7$), the use of more strongly electrically conducting fluids, such as liquid metals, are required to examine magnetoconvection (or dynamos) in laboratory experiments. Although in the planetary setting on icy satellites, salt water is a viable fluid for dynamo action (Gissinger & Petitdemange, 2019). Liquid metals typically have $Pr \ll 1$ and the results in this section include experiments using mercury ($Pr = 0.025$; Cioni et al., 2000), a sodium potassium alloy ($Pr \approx 0.02$; Burr & Müller, 2001), and liquid gallium ($Pr = 0.023$; Aurnou & Olson, 2001). The ratio of the thermal and magnetic Prandtl numbers $Pr : Pm$ dictates whether the onset of convection is steady or oscillatory for magnetoconvection (Chandrasekhar, 1961). Quasi-static magnetoconvection with steady onset, where $Pr \geq Pm$ and $Pm \ll 1$, is considered here as it is the relevant case for liquid metals and planetary cores. Stellar interiors where $Pr \lesssim Pm$ remain a greater challenge and much less is understood (Tobias, 2019).

Magnetoconvection without rotation is typically investigated by varying the Chandrasekhar number $Q = B^2H^2/\nu\mu\eta\rho$. This measures the ratio of magnetic forces to viscous forces. Linear analysis of the magnetoconvection problem indicates that the critical Rayleigh number Ra_{c_m} increases with the strength of the imposed field as measured by Q (Chandrasekhar, 1961), thereby indicating that the addition of magnetic fields inhibits convection. With no rotation and an asymptotically strong imposed magnetic field, the critical $Ra_{c_m} = \pi^2 Q$ (Chandrasekhar, 1961). Experimental results for heat transport in magnetoconvection are illustrated in Figure 4. A comparison with Figure 1 highlights the difficulties in exploring a large range of parameter space for constrained flows. Here the convection is constrained by the imposed magnetic field, which alters the supercriticality to depend on the magnetic field strength through Q. For an imposed magnetic field strength strong enough to influence the flow in the accessible range of Ra, the supercriticality Ra/Ra_{c_m} and Nusselt numbers are not far above the critical onset values of 1. However, scalings appear to exist in the regimes currently accessible (Aurnou & Olson, 2001; Cioni et al., 2000), indicating that these comparisons are worth pursuing.

The functional form

$$Nu = c_3 Pr^{\gamma}\left(\frac{Ra}{Ra_{c_m}}\right)^{\alpha} \tag{20}$$

in combination with this critical Rayleigh dependence can now be expressed as

$$q \propto \left(\frac{\kappa \Delta T}{H}\right)\left(\frac{\nu}{\kappa}\right)^{\gamma}\left(\frac{g\alpha_T \Delta T H^3}{\kappa \nu}\right)^{\alpha}\left(\frac{\nu \mu \eta \rho}{B^2 H^2}\right)^{\alpha}. \tag{21}$$

Assuming as before that the turbulent interior for sufficiently strong Ra becomes independent of κ and ν results in $-1 = -\alpha - \gamma$ and $0 = \gamma + \alpha - \alpha$. This is satisfied as $\gamma = 0$ and $\alpha = 1$, a result independent of Pr. Recent numerical simulations of magnetoconvection conducted at the highest values of Q support this finding (Yan et al., 2019). While this scaling is independent of thermal and viscous dissipation, it remains dependent on magnetic diffusivity. For low Pm regimes where $\nu \ll \eta$ it may thus be concluded that ohmic dissipation remains influential on the scales of convective motions. The functional form (20) does not explicitly contain a scaling dependence on Pm. However, we note that such an inclusion along with similar attempts to produce a dissipation-free analysis results in an inconsistent system of algebraic equations with no solution. Moreover, a dissipation-free scaling law separating the power law dependence of Ra, Q, Pr, and Pm results in $Nu \propto Pr^{1-\alpha}(RaPm/Q)^{\alpha}(Q/Pm)^{1/2}$ with α as an undetermined exponent. For fixed supercriticality this results in a strong $Nu \propto (Q/Pm)^{1/2}$ dependence that is not observed.

An argument following Priestley (1959) about the independence of the result to the layer depth also results in $\alpha = 1$. A third argument akin to Malkus (1954) uses a marginal stability analysis with boundary layers satisfying, given $Ra_{\lambda c_m} = \pi^2 Q_{\lambda}$,

$$\frac{Ra_{\lambda}}{Ra_{\lambda c_m}} = \left(\frac{\Delta T_{\lambda}}{\Delta T}\right)\left(\frac{\lambda}{H}\right)\frac{Ra}{\pi^2 Q} \equiv 1, \quad Q_{\lambda} = Q\left(\frac{\lambda}{H}\right)^2, \quad Nu_{\lambda} = \left(\frac{\Delta T}{\Delta T_{\lambda}}\right)\left(\frac{\lambda}{H}\right)Nu \equiv 1, \tag{22}$$

resulting in

$$Nu = \left(\frac{\Delta T_{\lambda}}{\Delta T}\right)\left(\frac{Ra}{\pi^2 Q}\right)^{1}. \tag{23}$$

If $\Delta T_{\lambda} \sim \Delta T$, then one retrieves the result of Cioni et al. (2000). However, this provides an upper bound if, as in rotating convection, the normalized temperature drop $\Delta T_{\lambda}/\Delta T$ is a decreasing function of Ra/Ra_{c_m}.

4.1. Inclusion of Rotation

When rotation is included along with the imposed magnetic field, the Elsasser number $\Lambda = \sigma B^2/\rho\Omega$ emerges as an additional nondimensional parameter. The Elsasser number measures the ratio of the Coriolis to Lorentz terms and can also be expressed as $\Lambda = EQ$. Thus, Λ provides a measure of the dominance of either the rotation or imposed magnetic field for the flow and varies as $E \to 0$ or $Q \to \infty$. This effect is evident in the dependence of the critical Rayleigh number for rotating magnetoconvection $Ra_{c_{rm}}(\Lambda)$. Varying with Λ, $Ra_{c_{rm}}(\Lambda = 0) \propto E^{-4/3}$ as for nonmagnetic rotating convection. For $0 < \Lambda \leq 1$, $Ra_{c_{rm}}$ decreases with increasing Λ until it reaches a minimum at $\Lambda = 1$, after which point $Ra_{c_{rm}}$ increases with increased Λ (Chandrasekhar, 1961).

Numerical and experimental studies (Aurnou & Olson, 2001; Stellmach & Hansen, 2004) of rotating magnetoconvection have shown that the interplay of the rotation and magnetic field has a strong effect on both the critical thermal forcing and convection, but it is not yet well understood. For $\Lambda = O(1)$, the magnetic field can act to facilitate convection (King & Aurnou, 2015; Yadav et al., 2015), requiring less heat input than nonmagnetic rotating flow to drive convection. However, the appropriate ansatz for the heat transfer scaling is not known. At the extremes of strong rotation or strong magnetic field, the flow reverts to either the magnetoconvection without rotation or the rotating convection with no magnetic field, both of which have been previously discussed. More work is needed in mapping out parameter space to determine the critical Rayleigh number relationship and explore rotating magnetoconvection scalings away from those extremes. Efforts in this area include pushing numerical codes to lower E and investigating larger areas of parameter space with simulations (Stellmach & Hansen, 2004). There has also been progress in using asymptotic

models to study magnetoconvection in the rapidly rotating limit that will allow for exploration of regime closer to geophysically relevant parameters (Calkins et al., 2015). This model uses a derivation based on the extreme size of the rotation parameters in the GAFD parameter regimes but incorporates the Lorentz forces into the expansion.

5. Discussion

The turbulent flows in planetary interiors and stars present a challenge for numerical and laboratory studies. They are typically characterized a large range of scales and current attempts to simulate these settings are limited to regimes that are orders of magnitude away from reality. To circumvent these limitations, researchers search for scaling laws to relate key dynamics in the flow. Scaling laws allow for extrapolation from results in a limited parameter space to a geophysically relevant parameter regime, thereby allowing for a better understanding of geophysical flows.

We focus in this brief review on the scaling laws for heat transport within thermally driven convection in the Rayleigh-Bénard system. The simplified system of RBC is an ideal candidate for both the search for scaling laws analytically and the verification of scaling laws through simulations. There are many dynamics that are neglected in plane layer RBC, including compressibility, curvature in the geometry, and dependence of fluid properties on thermodynamic state variables (non-Boussinesq) effects. These all may play a role in the scalings in geophysical and astrophysical objects; however, we focus here on RBC. The Rayleigh-Bénard system investigates the fundamental dynamic of convection, which is a driving force for many geophysical flows, and one of the key results from the system is the efficiency of the heat transfer. Despite the idealizations made in the RBC system, it is still not possible to achieve geophysically relevant Ra numbers either in the laboratory or numerical simulation. The search for scaling laws is motivated by the goal of characterizing the heat transfer in more strongly forced settings that are not accessible in simulation. The behavior of the heat transfer is closely linked to the underlying convection of the system and can provide insight into the types and transitions of flow structures as well as insight into the importance of boundary layers (e.g., Cheng et al., 2015; Christensen, 2010; King et al., 2010). Of course, the extrapolation of even carefully controlled numerical simulation and laboratory experiments should be carefully considered.

Building on the functional relationship $Nu \propto (Ra/Ra_c)^{\alpha}$ has led to key analytical predictions in fields where the critical Rayleigh number as a function of the input parameters is well understood. In each of the settings investigated here, namely, convection, rotating convection, and magnetoconvection, the scaling is explored using the ideas of either (i) a turbulent interior where the Nu, Ra relation is independent of dissipation, (ii) a Nu, Ra relation that is independent of the layer depth following Priestley (1959), or (iii) an analysis of marginally stable thermal boundary layers following Malkus (1954). In each case, the premise is that the mechanism with the smallest exponent forms the bottleneck in heat transport. The focus on the scalings has led to many advances within the RBC community, including bolstering progress through comparison, pointing to the importance of previously neglected physics, and allowing for more accurate extrapolation to unreachable regimes.

For RBC, $Ra_c = c$ combined with these scaling theories yields both an $\alpha = 1/3$ result and an scaling of $\alpha = 1/2$. Given that $1/3 < 1/2$, the heat transport is controlled by the boundary layer.

In the rotating RBC regime, $Ra_{c_r} \propto E^{-4/3}$ (Chandrasekhar, 1961) produces the scaling of $\alpha = 3/2$ and $\alpha = 3$. Since $3/2 < 3$, it is the dissipation-free interior dictating the heat transport, in contrast to nonrotating convection. Extensive numerical and experimental simulation (e.g., Cheng et al., 2015; King et al., 2012; Kunnen et al., 2016; Plumley et al., 2016; Sprague et al., 2006; Stellmach et al., 2014) have shown different scalings for different boundary conditions, although asymptotic model results indicate that for low E the $\alpha = 3/2$ scaling is dominant for all conditions (Plumley et al., 2017).

In magnetoconvection, the critical Rayleigh $Ra_{c_m} = \pi^2 Q$ (Chandrasekhar, 1961) is known for asymptotically large Q. An exponent of $\alpha = 1$ is achieved for all scaling arguments indicating that neither the interior nor boundary layers throttle the heat transfer significantly compared to the other. This scaling has been seen in experimental results from Cioni et al. (2000). The rotating magnetoconvection problem lacks a known $Ra_{c_{rm}}(\Lambda)$, which complicates the search for the heat transport scalings. Understanding the scalings in this setting, along with even more involved settings such as self-consistent dynamos, remains open.

Acknowledgments
The authors gratefully acknowledge funding from an ETH Zürich Postdoctoral Fellowship (M. P.) and NSF EAR1620649 (K. J.). All data used in this manuscript have been previously published in the cited works.

References

Ahlers, G., Bodenschatz, E., & He, X. (2017). Ultimate-state transition of turbulent Rayleigh-Bénard convection. *Physical Review Fluids*, *2*(5), 54603.
Ahlers, G., Grossmann, S., & Lohse, D. (2009). Heat transfer and large scale dynamics in turbulent Rayleigh-Bénard convection. *Reviews of modern physics*, *81*(2), 503.
Ahlers, G., & Xu, X. (2001). Prandtl-number dependence of heat transport in turbulent Rayleigh-Bénard convection. *Physical review letters*, *86*(15), 3320.
Aubert, J. (2019). Approaching Earth's core conditions in high-resolution geodynamo simulations. *Geophysical Journal International*, *219*(Supp. 1), S137–S151. https://doi.org/10.1093/gji/ggz232
Aurnou, J. M., Calkins, M. A., Cheng, J. S., Julien, K., & King, E. M. (2015). Rotating convective turbulence in Earth and planetary cores. *Physics of the Earth and Planetary Interiors*, *246*, 51–71.
Aurnou, J., & Olson, P. (2001). Experiments on Rayleigh–Bénard convection, magnetoconvection and rotating magnetoconvection in liquid gallium. *Journal of Fluid Mechanics*, *430*, 283–307.
Berhanu, M., Verhille, G., Boisson, J., Gallet, B., Gissinger, C., Fauve, S., et al. (2010). Dynamo regimes and transitions in the VKS experiment. *The European Physical Journal B*, *77*(4), 459–468.
Böhm-Vitense, E. (1958). About the hydrogen convection zone in stars of different effective temperatures and luminosities. *Journal of Astrophysics*, *46*, 108.
Bouillaut, V., Lepot, S., Aumaître, S., & Gallet, B. (2019). Transition to the ultimate regime in a radiatively driven convection experiment. *Journal of Fluid Mechanics*, *861*, R5.
Burr, U., & Müller, U. (2001). Rayleigh–Bénard convection in liquid metal layers under the influence of a vertical magnetic field. *Physics of Fluids*, *13*(11), 3247–3257.
Busse, F. (1981). Transition to turbulence in thermal convection with and without rotation, *Transition and turbulence* (pp. 43–61). New York: Academic Press.
Calkins, M. A., Julien, K., Tobias, S. M., & Aurnou, J. M. (2015). A multiscale dynamo model driven by quasi-geostrophic convection. *Journal of Fluid Mechanics*, *780*, 143–166.
Cattaneo, F., & Hughes, D. W. (2006). Dynamo action in a rotating convective layer. *Journal of Fluid Mechanics*, *553*, 401–418.
Chandrasekhar, S. (1961). *Hydrodynamic and hydromagnetic stability*. Oxford: Oxford University Press.
Cheng, J. S., Aurnou, J. M., Julien, K., & Kunnen, R. P. J. (2018). A heuristic framework for next-generation models of geostrophic convective turbulence. *Geophysical and Astrophysical Fluid Dynamics*, *112*, 277–300.
Cheng, J. S., Stellmach, S., Ribeiro, A., Grannan, A., King., E. M., & Aurnou, J. M. (2015). Laboratory-numerical models of rapidly rotating convection in planetary cores. *Geophysical Journal International*, *201*, 1–17.
Chillà, F., & Schumacher, J. (2012). New perspectives in turbulent Rayleigh-Bénard convection. *The European Physical Journal E*, *35*(7), 58.
Christensen, U. (2010). Dynamo scaling laws and applications to the planets. *Space Science Reviews*, *152*(1-4), 565–590.
Christensen, U. R., & Aubert, J. (2006). Scaling properties of convection-driven dynamos in rotating spherical shells and application to planetary magnetic fields. *Geophysical Journal International*, *166*(1), 97–114.
Cioni, S., Chaumat, S., & Sommeria, J. (2000). Effect of a vertical magnetic field on turbulent Rayleigh-Bénard convection. *Physical Review E*, *62*(4), R4520.
Constantin, P., & Doering, C. R. (1999). Infinite Prandtl number convection. *Journal of Statistical Physics*, *94*(1-2), 159–172.
Cross, M. C., & Hohenberg, P. C. (1993). Pattern formation outside of equilibrium. *Reviews of modern physics*, *65*(3), 851.
Davidson, P. (2013). Scaling laws for planetary dynamos. *Geophysical Journal International*, *195*(1), 67–74.
Doering, C. R., & Constantin, P. (1996). Variational bounds on energy dissipation in incompressible flows. III. Convection. *Physical Review E*, *53*(6), 5957.
Doering, C., Wettlaufer, J., & Toppaladoddi, S. (2018). Absence of evidence for transition to the "ultimate" regime of Rayleigh-Bénard convection. *Bulletin of the American Physical Society*, *63*.
Ecke, R. E., & Niemela, J. J. (2014). Heat transport in the geostrophic regime of rotating Rayleigh-Bénard convection. *Physical Review Letters*, *113*, 114301.
Fauve, S., & Petrelis, F. (2003). The dynamo effect. *Peyresq lectures on Nonlinear phenomena*, *2*, 1–64.
Funfschilling, D., Brown, E., Nikolaenko, A., & Ahlers, G. (2005). Heat transport by turbulent Rayleigh–Bénard convection in cylindrical samples with aspect ratio one and larger. *Journal of Fluid Mechanics*, *536*, 145–154.
Gastine, T., Wicht, J., & Aubert, J. (2016). Scaling regimes in spherical shell rotating convection. *Journal of Fluid Mechanics*, *808*, 690–732.
Gissinger, C., & Petitdemange, L. (2019). A magnetically driven equatorial jet in Europa's ocean. *Nature Astronomy*, *3*, 401–407.
Grooms, I. (2015). Asymptotic behavior of heat transport for a class of exact solutions in rotating Rayleigh–Bénard convection. *Geophysical & Astrophysical Fluid Dynamics*, *109*(2), 145–158.
Grooms, I., & Whitehead, J. P. (2014). Bounds on heat transport in rapidly rotating Rayleigh–Bénard convection. *Nonlinearity*, *28*(1), 29.
Grossmann, S., & Lohse, D. (2001). Thermal convection for large Prandtl numbers. *Physical review letters*, *86*(15), 3316.
Grossmann, S., & Lohse, D. (2002). Prandtl and Rayleigh number dependence of the Reynolds number in turbulent thermal convection. *Physical Review E*, *66*(1), 16305.
Guervilly, C., Cardin, P., & Schaeffer, N. (2019). Turbulent convective length scale in planetary cores. *Nature*, *570*(7761), 368.
He, X., Funfschilling, D., Nobach, H., Bodenschatz, E., & Ahlers, G. (2012). Transition to the ultimate state of turbulent Rayleigh-Bénard convection. *Physical Review Letters*, *108*, 24502.
Horn, S., & Aurnou, J. M. (2018). Regimes of Coriolis-Centrifugal Convection. *Physical Review Letters*, *120*, 204502.
Howard, L. N. (1972). Bounds on flow quantities. *Annual Review of Fluid Mechanics*, *4*(1), 473–494.
Jones, C. (2007). Thermal and compositional convection in the outer core. *Treatise in Geophysics, Core Dynamics*, *8*, 131–185.
Jones, C. A. (2011). Planetary magnetic fields and fluid dynamos. *Annual Review of Fluid Mechanics*, *43*, 583–614.
Julien, K., Aurnou, J., Calkins, M., Knobloch, E., Marti, P., Stellmach, S., & Vasil, G. (2016). A nonlinear model for rotationally constrained convection with Ekman pumping. *Journal of Fluid Mechanics*, *798*, 50–87.
Julien, K., & Knobloch, E. (1998). Strongly nonlinear convection cells in a rapidly rotating fluid layer: The tilted *f*-plane. *Journal of Fluid Mechanics*, *360*, 141–178.
Julien, K., & Knobloch, E. (2007). Reduced models for fluid flows with strong constraints. *Journal of Mathematical Physics*, *48*(6), P065405.
Julien, K., Knobloch, E., Milliff, R., & Werne, J. (2006). Generalized quasi-geostrophy for spatially anistropic rotationally constrained flows. *Journal of Fluid Mechanics*, *555*, 233–274.

Julien, K., Rubio, A. M., Grooms, I., & Knobloch, E. (2012). Statistical and physical balances in low Rossby number Rayleigh-Bénard convection. *Geophysical & Astrophysical Fluid Dynamics*, *106*(4-5), 392–428.
King, E. M., & Aurnou, J. M. (2013). Turbulent convection in liquid metal with and without rotation. *Proceedings of the National Academy of Sciences*, *110*(17), 6688–6693.
King, E. M., & Aurnou, J. M. (2015). Magnetostrophic balance as the optimal state for turbulent magnetoconvection. *Proceedings of the National Academy of Sciences*, *112*(4), 990–994.
King, E. M., Soderlund, K. M., Christensen, U. R., Wicht, J., & Aurnou, J. M. (2010). Convective heat transfer in planetary dynamo models. *Geochemistry, Geophysics, Geosystems*, *11*, Q06016. https://doi.org/10.1029/2010GC003053
King, E. M., Stellmach, S., & Aurnou, J. M. (2012). Heat transfer by rapidly rotating Rayleigh-Bénard convection. *Journal of Fluid Mechanics*, *691*, 568–582.
Kraichnan, R. H. (1962). Turbulent thermal convection at arbitrary Prandtl number. *The Physics of Fluids*, *5*(11), 1374–1389.
Kunnen, R., Clercx, H., & Van Heijst, G. (2013). The structure of sidewall boundary layers in confined rotating Rayleigh–Bénard convection. *Journal of fluid mechanics*, *727*, 509–532.
Kunnen, R. P. J., Ostilla-Mnico, R., van der Poel, E. P., Verzicco, R., & Lohse, D. (2016). Transition to geostrophic convection: The role of the boundary conditions. *Journal of Fluid Mechanics*, *799*, 413–432.
Lathrop, D. P., & Forest, C. B. (2011). Magnetic dynamos in the lab. *Physics Today*, *64*(7), 40–45.
Liu, W., Krasnov, D., & Schumacher, J. (2018). Wall modes in magnetoconvection at high Hartmann numbers. *Journal of Fluid Mechanics*, *849*, R2.
Lohse, D., & Toschi, F. (2003). Ultimate state of thermal convection. *Physical review letters*, *90*(3), 34502.
Malkus, W. V. R. (1954). The heat transport and spectrum of thermal turbulence. *Proceedings of the Royal Society of London. Series A*, *225*(1161), 196–212. https://doi.org/10.1098/rspa.1954.0197
Miesch, M. S. (2005). Large-scale dynamics of the convection zone and tachocline. *Living Reviews in Solar Physics*, *2*(1), 1.
Moore, G. E. (1965). Cramming more components onto integrated circuits. *Electronics Magazine*, *38*(8), 114–117.
Niemela, J., Skrbek, L., Sreenivasan, K., & Donnelly, R. (2000). Turbulent convection at very high Rayleigh numbers. *Nature*, *404*(6780), 837.
Niiler, P. P., & Bisshopp, F. E. (1965). On the influence of the Coriolis force on onset of thermal convection. *Journal of Fluid Mechanics*, *22*, 753–761.
Plumley, M., Julien, K., Marti, P., & Stellmach, S. (2016). The effects of Ekman pumping on quasi-geostrophic Rayleigh-Bénard convection. *Journal of Fluid Mechanics*, *803*, 51–71. https://doi.org/10.1017/jfm.2016.452
Plumley, M., Julien, K., Marti, P., & Stellmach, S. (2017). Sensitivity of rapidly rotating Rayleigh-Bénard convection to Ekman pumping. *Physical Review Fluids*, *2*, 94801.
Pope, S. (2000). *Turbulent flows*. Cambridge, United Kingdom: Cambridge University Press.
Priestley, C. H. B. (1959). *Turbulent transfer in the lower atmosphere*. Chicago: University of Chicago Press.
Roche, P.-E., Castaing, B., Chabaud, B., & Hébral, B. (2002). Prandtl and Rayleigh numbers dependences in Rayleigh-Bénard convection. *EPL (Europhysics Letters)*, *58*(5), 693.
Rossby, H. (1969). A study of Bénard convection with and without rotation. *Journal of Fluid Mechanics*, *36*(2), 309–335.
Rubio, A. M., Julien, K., Knobloch, E., & Weiss, J. B. (2014). Upscale energy transfer in three-dimensional rapidly rotating turbulent convection. *Physical Review Letters*, *112*, 144501.
Schubert, G., & Soderlund, K. M. (2011). Planetary magnetic fields: Observations and models. *Physics of Earth & Planetary Interiors*, *187*(3), 92–108.
Shraiman, B. I., & Siggia, E. D. (1990). Heat transport in high-Rayleigh-number convection. *Physical Review A*, *42*(6), 3650.
Spiegel, E. A. (1971). Convection in stars I. Basic Boussinesq convection. *Annual review of astronomy and astrophysics*, *9*(1), 323–352.
Sprague, M., Julien, K., Knobloch, E., & Werne, J. (2006). Numerical simulation of an asymptotically reduced system for rotationally constrained convection. *Journal of Fluid Mechanics*, *551*, 141–174.
Stellmach, S., & Hansen, U. (2004). Cartesian convection driven dynamos at low Ekman number. *Physical Review E*, *70*(5), 56312.
Stellmach, S., Lischper, M., Julien, K., Vasil, G., Cheng, J. S., Ribeiro, A., et al. (2014). Approaching the asymptotic regime of rapidly rotating convection: Boundary layers versus interior dynamics. *Physical Review Letters*, *113*, 254501.
Stevens, R. J., Lohse, D., & Verzicco, R. (2011). Prandtl and Rayleigh number dependence of heat transport in high Rayleigh number thermal convection. *Journal of fluid mechanics*, *688*, 31–43.
Sun, C., Ren, L.-Y., Song, H., & Xia, K.-Q. (2005). Heat transport by turbulent Rayleigh–Bénard convection in 1 m diameter cylindrical cells of widely varying aspect ratio. *Journal of Fluid Mechanics*, *542*, 165–174.
Thual, O. (1992). Zero-Prandtl-number convection. *Journal of Fluid Mechanics*, *240*, 229–258.
Tilgner, A. (2012). Transitions in rapidly rotating convection driven dynamos. *Physical Review Letters*, *109*(24), 248501.
Tobasco, I., & Doering, C. R. (2017). Optimal wall-to-wall transport by incompressible flows. *Physical Review Letters*, *118*(26), 264502.
Tobias, S. (2019). The turbulent dynamo. arXiv preprint arXiv:1907.03685.
Wang, X. (2004). Infinite Prandtl number limit of Rayleigh-Bénard convection. *Communications on Pure and Applied Mathematics: A Journal Issued by the Courant Institute of Mathematical Sciences*, *57*(10), 1265–1282.
Whitehead, J. P., & Doering, C. R. (2011). Ultimate state of two-dimensional Rayleigh-Bénard convection between free-slip fixed-temperature boundaries. *Physical Review Letters*, *106*(24), 244501.
Yadav, R. K., Gastine, T., Christensen, U. R., Duarte, L., & Reiners, A. (2015). Effect of shear and magnetic field on the heat-transfer efficiency of convection in rotating spherical shells. *Geophysical Journal International*, *204*(2), 1120–1133.
Yan, M., Calkins, M. A., Maffei, S., Julien, K., Tobias, S. M., & Marti, P. (2019). Heat transfer and flow regimes in quasi-static magnetoconvection with a vertical magnetic field. arXiv preprint arXiv:1905.13688.
Zhu, X., Mathai, V., Stevens, R. J., Verzicco, R., & Lohse, D. (2018). Transition to the ultimate regime in two-dimensional Rayleigh-Bénard convection. *Physical Review Letters*, *120*(14), 144502.
Zimmerman, D. S., Triana, S. A., Nataf, H.-C., & Lathrop, D. P. (2014). A turbulent, high magnetic Reynolds number experimental model of Earth's core. *Journal of Geophysical Research: Solid Earth*, *119*, 4538–4557. https://doi.org/10.1002/2013JB010733